iScience

CellPress
OPEN ACCESS

Article

Mesenchymal stem cell-derived small extracellular vesicles alleviate the immunometabolic dysfunction in murine septic encephalopathy

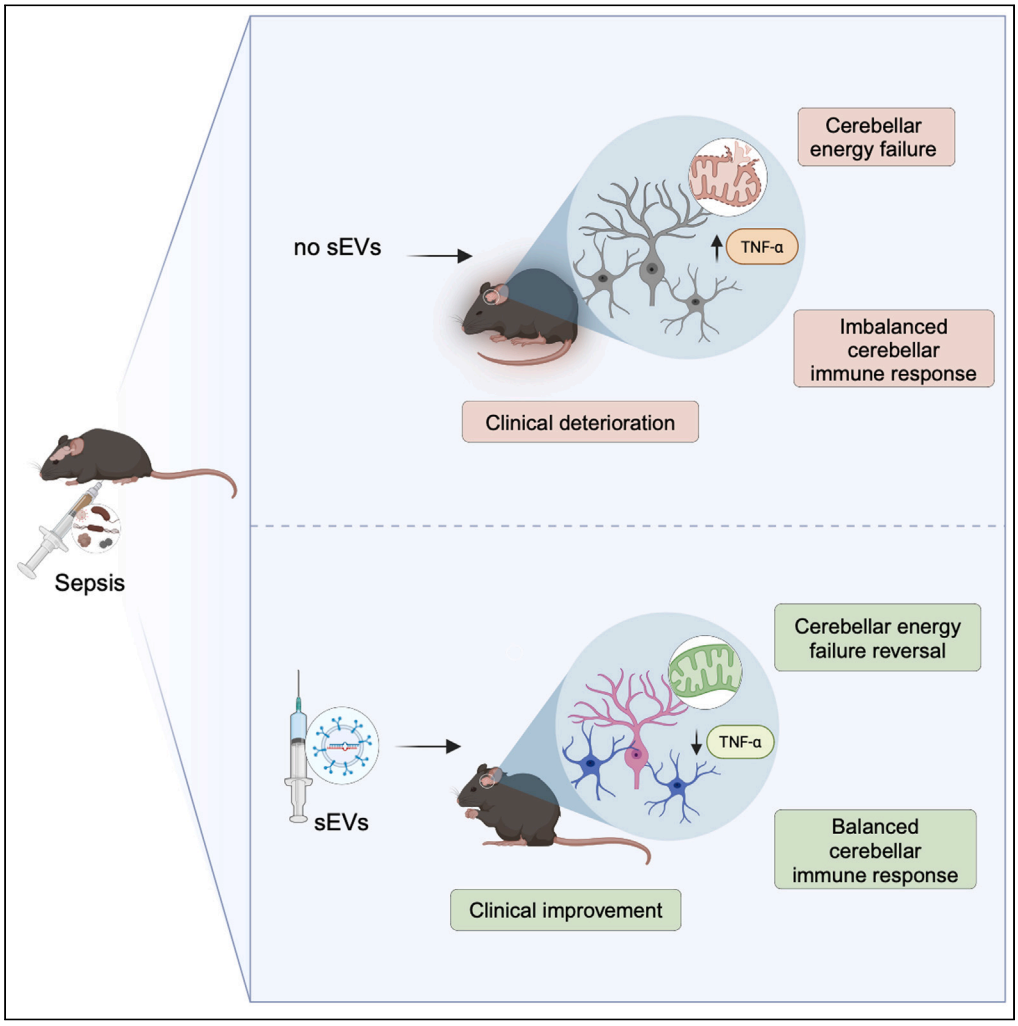

Ioannis Koutroulis, Panagiotis Kratimenos, Claire Hoptay, ..., Manish Bharadwaj, Vittorio Gallo, Robert Freishtat

ikoutrouli@childrensnational.org

Highlights

Septic encephalopathy (SE) leads to notable immunometabolic damage in murine cerebellum

Cerebellar injury in SE is associated with immune imbalance and an energy deficit

MSC-derived sEV administration leads to clinical improvement of SE symptoms

MSC-derived sEV treatment reverses many of the immune and metabolic changes caused by SE

Koutroulis et al., iScience 27, 110573
August 16, 2024
https://doi.org/10.1016/j.isci.2024.110573

iScience

CellPress
OPEN ACCESS

Article

Mesenchymal stem cell-derived small extracellular vesicles alleviate the immunometabolic dysfunction in murine septic encephalopathy

Ioannis Koutroulis,[1,2,4,8,*] Panagiotis Kratimenos,[2,3,4] Claire Hoptay,[4] Wade N. O'Brien,[5] Georgios Sanidas,[4] Chad Byrd,[4] Maria Triantafyllou,[4] Evan Goldstein,[6] Beata Jablonska,[4] Manish Bharadwaj,[7] Vittorio Gallo,[2,4] and Robert Freishtat[1,2,4]

SUMMARY

Sepsis is a life-threatening organ dysfunction caused by a dysregulated host response to infection that results in high mortality and long-term sequela. The central nervous system (CNS) is susceptible to injury from infectious processes, which can lead to clinical symptoms of septic encephalopathy (SE). SE is linked to a profound energetic deficit associated with immune dysregulation. Here, we show that intravenous administration of adipose tissue mesenchymal stem cell (MSC)-derived small extracellular vesicles (sEVs) in septic mice improved disease outcomes by reducing SE clinical severity, restoring aerobic metabolism, and lowering pro-inflammatory cytokines in the cerebellum, a key region affected by SE. Our high throughput analysis showed that MSC-derived sEVs partially reversed sepsis-induced transcriptomic changes, highlighting the potential association of miRNA regulators in the cerebellum of MSC-derived sEV-treated mice with miRNAs identified in sEV cargo. MSC-derived sEVs could serve as a promising therapeutic agent in SE through their favorable immunometabolic properties.

INTRODUCTION

Sepsis, a clinical syndrome that is involved in up to 20% of deaths worldwide, can affect almost all organs, and is characterized by an imbalance between a hyperimmune response and immunoparalysis secondary to an infectious process.[1–5] The central nervous system (CNS) is one of the organs susceptible to injury from sepsis, leading to septic encephalopathy (SE).[3,6] In SE, the cerebellum sustains significant damage with neuronal cell death secondary to immune-mediated neuroinflammation.[7,8] In addition to immune-mediated neuroinflammation, a few studies have described sepsis-associated energy deficit as an additional contributor to septic organ dysfunction.[9–12] Sepsis shifts cells from energy-efficient mitochondrial oxidative phosphorylation (OXPHOS) to glycolysis, resulting in an almost 20-fold reduction in cellular ATP.[4–6] Overall energy deficiency leads to accumulation of reactive oxygen species (ROS), oxidative stress, and cell apoptosis with subsequent organ failure and increased mortality risk.[11,12] While evidence suggests that this energy deficit activates immune-mediated neuroinflammation and apoptosis in the brain,[13,14] the contribution of a concurrent sepsis-related immune and metabolic dysfunction to SE pathophysiology is not fully understood.

To date, no sepsis treatments address both immune dysfunction and energetics, together known as immunometabolism. However, mesenchymal stem cells (MSCs) show beneficial effects on immunometabolism in several clinical conditions that are related to sepsis, such as acute respiratory distress syndrome (ARDS) and bacterial pneumonia.[5,15,16] MSC effects are partially facilitated by the transfer of mitochondria to innate immune cells, which promote restoration of energetics by improving OXPHOS and redox homeostasis.[16,17] Moreover, Matthay et al. showed that MSC-derived small extracellular vesicles (sEVs), 20–100 nm in size, might also be responsible for MSC-improved organ energetics via horizontal transfer of bioactive molecules.[18] Several reports have demonstrated the long-lasting immunometabolic benefits of MSC-derived sEVs.[17,19,20] Despite the ability of sEVs to cross the blood-brain barrier in mice and their favorable therapeutic potential, the mechanistic effects of MSC-derived sEVs in SE have not been investigated. Here, we use a murine model of polymicrobial sepsis with MSC-derived sEVs in a dual therapeutic role to address both immune dysfunction and energetics in SE. We hypothesize that a CNS energy

[1]Department of Pediatrics, Division of Emergency Medicine, Children's National Hospital, Washington, DC 20010, USA
[2]George Washington University School of Medicine and Health Sciences, Washington, DC 20010, USA
[3]Department of Pediatrics, Division of Neonatology, Children's National Hospital, Washington, DC 20010, USA
[4]Children's National Research Institute, Washington, DC 20010, USA
[5]Dartmouth College Geisel School of Medicine, Hanover, NH 03755, USA
[6]Augusta University Medical College of Georgia, Augusta, GA 30912, USA
[7]Agilent Inc, Santa Clara, CA 95051, USA
[8]Lead contact
*Correspondence: ikoutrouli@childrensnational.org
https://doi.org/10.1016/j.isci.2024.110573

deficit in SE induces immune pathways leading to neuroinflammation and neuronal cell death, which is mitigated by the administration of MSC-derived sEVs. In the present study we found that intravenous (IV) administration of adipose tissue-derived MSC-derived sEVs effectively counters these issues, leading to improved clinical outcomes. This is the first pre-clinical study utilizing MSC-derived sEVs as a therapeutic agent in SE.

RESULTS

MSC-derived sEVs improve clinical scores in murine polymicrobial sepsis

We used a murine model of sepsis in which mice develop polymicrobial peritonitis and sepsis via intraperitoneal (IP) injection of a slurry of cecal contents from donor mice. In mice, sepsis severity can be measured using a validated scoring system with observable and quantifiable parameters.[21] The scoring system includes seven components ranging from 0 to 4 points (0: normal, 4: most severe, maximum score: 28 points) related to general appearance, respiratory system, CNS function, and eye appearance (Table 1).[21] The mice became clinically septic at 10–12 h following sepsis induction with IP injection. We euthanized mice that reached a score of 15 or higher. All mice were euthanized regardless of their score at 24 h post-IP injections (Figure 1A).

We analyzed 26 septic mice in the MSC-derived sEV-treated group and 19 septic mice in the untreated group (i.e., treated with sEV-depleted media). Despite their comparable baseline severity scores at the time of treatment (6 h post-sepsis induction) (Mean $\pm$ SEM: 8.3 $\pm$ 0.5 in MSC-derived sEV-treated vs. 9.4 $\pm$ 0.6 in untreated mice, $p = 0.14$), the mean sepsis severity scores of the treated mice at the time of euthanasia (24 h post-sepsis induction) were significantly lower compared to untreated mice (12.1 $\pm$ 1.0 vs. 15.6 $\pm$ 1.0, $p = 0.0005$). We also compared the groups for the highest sepsis score reached (i.e., peak score), and found a lower peak score in MSC-derived sEV-treated compared to the untreated mice (12.6 $\pm$ 0.8 vs. 15.8 $\pm$ 0.8, $p < 0.0001$) (Figure 1B). However, when only the three CNS function-related scoring parameters (i.e., level of consciousness, general activity, and response to stimuli; maximum = 12) were assessed, there was no difference between groups in peak scores, while the MSC-derived sEV-treated septic mice were still improved compared to the untreated group at the time of euthanasia (7.2 $\pm$ 0.5 vs. 8.5 $\pm$ 0.2, $p = 0.01$) (Figure 1C).

Sepsis-induced cerebellar injury is attenuated by MSC-derived sEVs

Evidence supports that sEVs cross the blood-brain barrier (BBB), a property that is enhanced in acute inflammatory conditions such as sepsis.[22] First, we morphologically assessed the brain of mice 24 h after the induction of sepsis, and we identified that the cerebellum was the brain region most affected in early sepsis. In mice with sepsis ($n = 8$), the cerebellum displayed significant neuropathological alterations (perineuronal edema, cell death, chromatolysis) compared to non-septic controls ($n = 7$). We used a modified quantification scoring system ranging from 0 to 4 (0: no injury and 4: severe injury) (Hoque et al., 2014), which showed significant injury in the cerebellum of mice with sepsis compared to controls [Median score 3.0 (Maximum 4.0, Minimum 2.0) vs. 1.0 (Maximum 1.5, Minimum 0.0), $p < 0.0001$] and also to septic mice that received MSC-derived sEVs (Median score 2.0 (Max. 3.0, Min. 0.5) vs. 3.0 (Max. 4.0, Min. 2.0), $p = 0.0155$) (Figures 2A and 2C). Treatment with MSC-derived sEVs attenuated cerebellar injury and prevented perineuronal vacuole formation and rarefication of the neuropil (Figures 2A and 2C). We observed forms of cell death including apoptosis and necrosis, as well as hybrid forms of the cell death continuum. We used TUNEL staining to confirm cell death findings and the results were in line with the morphological assessment by H&E (Figures 2B and 2D); sepsis increased the number of TUNEL+ cells indicating cell death (8.1 $\pm$ 3.6 vs. 0.4 $\pm$ 0.2 cells/HPF, $p < 0.0001$), which was reversed by treatment with MSC-derived sEVs (5.4 $\pm$ 2.4 cells/HPF, $p = 0.0063$) (Figures 2B and 2D). Together, these data indicate that neuronal injury of the cerebellum induced by sepsis can be mitigated by treatment with MSC-derived sEVs.

Sepsis induces alterations in the cerebellar transcriptome

Building up on our findings on cerebellar neuropathology, we performed RNA sequencing to define the molecular changes underlying these observations. We compared differentially expressed genes (DEGs) among the four groups (DESeq2).[23] Distinct expression patterns were evident between MSC-derived sEV-treated and untreated septic mice and non-septic controls. Specifically, between untreated septic mice and non-septic controls, we noted a very high number (7,338 total, 3,668 downregulated, 3,670 upregulated) of DEGs. Direct comparison between septic MSC-derived sEV-treated and untreated mice revealed 222 total, 103 downregulated, and 119 upregulated DEGs.

Ingenuity Pathway Analysis (IPA; Qiagen, Germantown, MD) showed that pathways such as macrophage migration inhibitory factor (MIF) regulation of innate immunity, toll-like receptor signaling, tumor Necrosis Factor Receptor 1 (TNFR1), and interleukin 6 (IL-6) signaling were all predicted to be activated by sepsis (Figure 3B). Additionally, in septic group, the predicted activation of nuclear factor kappa B (NF-κB) and hypoxia-inducible factor 1 (HIF-1), highlight their critical role in modulating immune reactivity and metabolic adaptation, essential for combatting infection in septic states (Figure 3B). IPA analysis predicted activation of sepsis-induced immune response functions such as recruitment of phagocytes, neutrophils, myeloid cells, and granulocytes, and activation and cell movement of leukocytes (Figure 3C). These findings highlight the significance of neuronal inflammation in septic brain injury. We assessed specific markers implicated in neuroinflammation, particularly those related to microglial cell presence. Classical markers of microglial cells, including CX3CR1, IGF1, TGFBR1, alongside the activation marker TREM2, were activated by sepsis compared to controls. Conversely, treatment with sEVs suppressed the expression of these markers relative to the sepsis group. These findings affirm the presence of microglial cells in septic brain injury and suggest the potential for mitigation through sEVs treatment (Figure S1).

Table 1. Murine sepsis scoring system (adapted from Shrum et al.)

Variable	Score/Description
Appearance	0- Coat is smooth
	1- Patches of hair piloerected
	2- Majority of back is piloerected
	3- Piloerection may or may not be present, mouse appears "puffy"
	4- Piloerection may or may not be present, mouse appears emaciated
Level of consciousness	0- Mouse is active
	1- Mouse is active but avoids standing upright
	2- Mouse activity is noticeably slowed but the mouse is still ambulant
	3- Activity is impaired, the mouse moves only when provoked and movements have a tremor
	4- Activity severely impaired and the mouse remains stationary when provoked with possible tremor
Activity	0- Normal amount of activity. Mouse does any of the following: eating, drinking, climbing, running, fighting
	1- Slightly suppressed activity. Mouse is moving around bottom of cage
	2- Suppressed activity. Mouse is stationary with occasional investigative movements
	3- No activity. Mouse is stationary
	4- No activity. Mouse experiencing tremors, particularly in the hind legs
Response to stimulus	0- Mouse responds immediately to auditory stimulus or touch
	1- Slow or no response to auditory stimulus; strong response to touch (moves to escape)
	2- No response to auditory stimulus; moderate response to touch (moves a few steps)
	3- No response to auditory stimulus; mild response to touch (no locomotion)
	4- No response to auditory stimulus; little or no response to touch. Cannot right itself if pushed over
Eyes	0- Open
	1- Eyes not fully open, possibly with secretions
	2- Eyes at least half closed, possibly with secretions
	3- Eyes half closed or more, possibly with secretions
	4- Eyes closed or milky
Respiratory rate	0- Normal, rapid mouse respiration
	1- Slightly decreased respiration (rate not quantifiable by eye)
	2- Moderately reduced respiration (rate at the upper range of quantifying by eye)
	3- Severely reduced respiration (rate easily countable by eye, 0.5 s between breaths)
	4- Extremely reduced respiration (>1 s between breaths)
Quality of respiration	0- Normal
	1- Brief periods of labored breathing
	2- Labored, no gasping
	3- Labored with intermittent gasps
	4- Gasping

The system allows for pathophysiologic assessment of mice under septic conditions including CNS and respiratory systems.

The predicted activation of various CNS cells (including immune cells) and the lung damage pathway correlate well with the potential mechanism of cerebellar damage in SE, which involves immune activation leading to organ impairment (Figure 3C). Consistent with these findings, the cytokines interleukin-1 beta (IL-1β), IL-6, and Tumor Necrosis Factor alpha (TNF-α) were predicted to be upstream regulators dictating many of the DEGs after sepsis was induced (Figure 3D). Specific transcripts coding for IL-1 and IL-6 receptors and toll-like receptor 2 were upregulated in untreated septic mice but not in non-septic controls (Figure 3E).

In terms of energy production and utilization, fatty acid metabolism was predicted to be increased in sepsis to meet high energy demand. Among the pathways of the peroxisome proliferator-activated receptor (PPAR) family, only the PPARα/RXRα pathway was predicted to be activated, highlighting its crucial role in metabolism and lipid regulation, essential for maintaining metabolic and energy homeostasis. (Figure 3B). Type 1 diabetes mellitus and insulin receptor signaling were activated, likely to maintain glucose homeostasis and available energy (Figure 3B). Correspondingly, the significantly higher expression of the glucose transporter (SLC2A4) and glucose-6-phosphatase (G6PC)

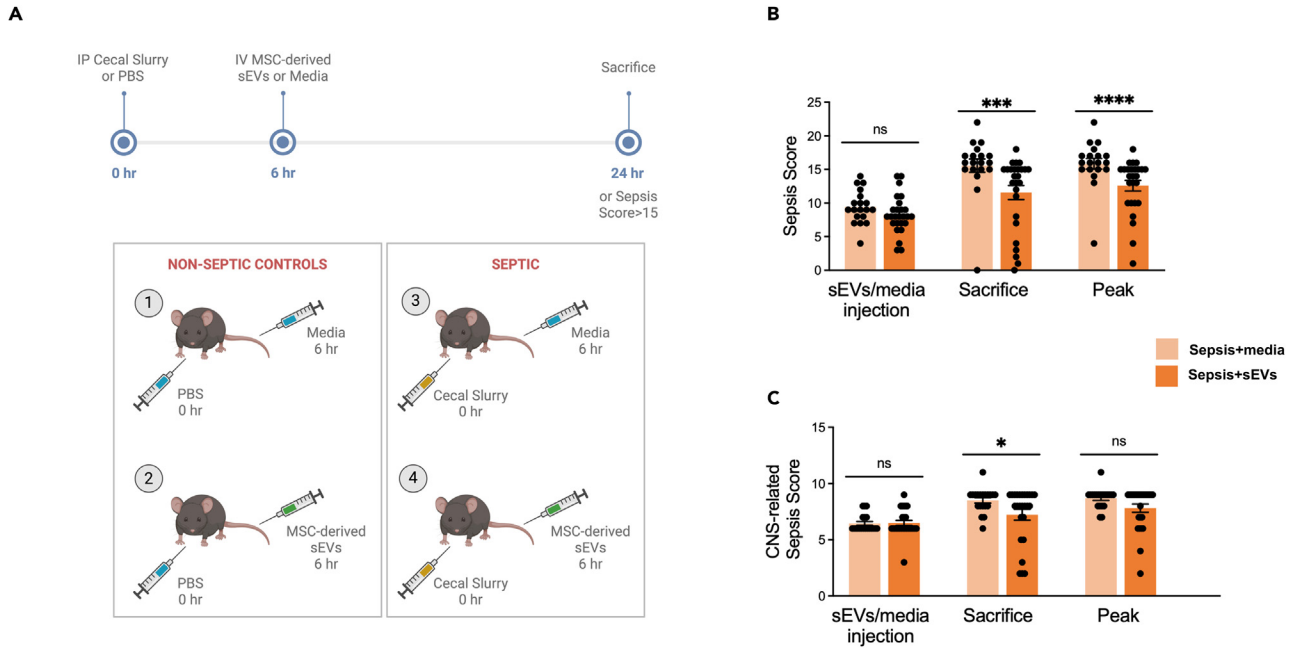

Figure 1. MSC-derived sEV treatment decreases clinical severity scores in murine sepsis

(A) Diagram of murine cecal slurry model. Mice were injected with cecal slurry IP, to induce polymicrobial sepsis. At 6 h post-injection, MSC-derived sEVs or sEV-depleted media were administered via tail vein injection. When mice reached a sepsis score of 15 or above or at 24 h post-IP injection, the brain tissue was harvested.

(B) MSC-derived sEV treatment (n = 26) in mice 6 h after the onset of sepsis resulted in improved disease overall severity score as compared with the untreated septic mice (n = 19) (***p = 0.0005) and lower peak scores (****$p < 0.0001$).

(C) MSC-derived sEV treatment improved scores at 24 h in neurological-only parameters (i.e., level of consciousness, activity, response to stimulus) as compared with the untreated septic mice (*p = 0.01). Data are represented as mean ± SEM, one-way ANOVA. ANOVA: Analysis of Variance, IP: intraperitoneally, MSC-derived sEV: mesenchymal stem cell-derived small extracellular vesicles, NS: non-significant.

genes in the septic group compared to non-septic controls supports this hypothesis (Figure 3E). In SE group, compared to controls, elevated gene expression of Neuroglobin (NGB) and Neuronal Pentraxin II (NPTX2) suggests protective roles against hypoxia and synaptic disruptions, respectively. Conversely, reduced gene expression of Fatty Acid Binding Protein 7, Brain (FABP7) indicates impaired neural metabolism, emphasizing the brain's vulnerability in sepsis. (Figure 3E).

The administration of MSC-derived sEVs in mice with SE strategically modulates genetic and signaling pathways to effectively manage both the systemic infection and its neurological consequences. Activation of the myeloid differentiation primary response 88 gene (MYD88) enhances the innate immune response, crucial for combating the underlying infection, supplemented by upregulation of the interleukin-17 alpha (IL-17α) receptor for a targeted immune response beneficial within the CNS (Figure 4A). Concurrently, activation of pathways including peroxisome proliferator-activated receptor gamma coactivator 1-alpha (PPARGC1A) boosts mitochondrial function, while insulin-like growth factor 1 (IGF-1), phosphatidylinositol 3-kinase/protein kinase B (PI3K/AKT), and CREB signaling pathways support neuronal growth, survival, plasticity, and protection,[24] enhancing brain resilience against sepsis (Figures 4A and 4B). Also, activation of the Dopamine-DARPP32 feedback in cAMP signaling pathway, is a key player in the response to dopamine and glutamate of the GABAergic medium-size spiny neurons[25] promoting the survival and plasticity of neuronal cells in the treated group (Figure 4B). Neutrophil migration and immune cell proliferation pathways are activated, in the treatment group, indicating immune modulation that optimizes recovery while maintaining neuronal integrity (Figure 4C). Glucose transporter (SLC2A12) downregulation after MSC-derived sEV administration may be a mechanism to prevent sepsis-induced hyperglycemia (Figure 4A). In the treatment group, (IL-6) signaling was inhibited, and interleukin-10 (IL-10) was downregulated, along with (IL-1) receptors, thereby reducing inflammation and preserving neuronal functions (Figures 4A, 4B, and 4D). This approach highlights the potential of MSC-derived EVs to manage systemic sepsis and specifically mitigate the complex events in SE, balancing brain function preservation with systemic inflammation control.

MSC-derived sEVs prevent glia-associated cytokine imbalance in septic murine cerebellum

To investigate the RNA-seq data from septic mice that showed a relative enrichment of immunometabolic pathways in greater detail, we used immunostaining to label for markers of gliosis and inflammatory cytokines. We hypothesized that the observed perineuronal vacuoles are due to gliosis and indeed labeling with GFAP confirmed the presence of reactive astrocytes in sepsis which surrounded the somata of Purkinje cells (PCs) and their dendrites within the molecular layer (44.17 ± 4.53 vs. 0.83 ± 0.54, $p < 0.0001$), (Figures S2A and S2B). Treatment with sEVs

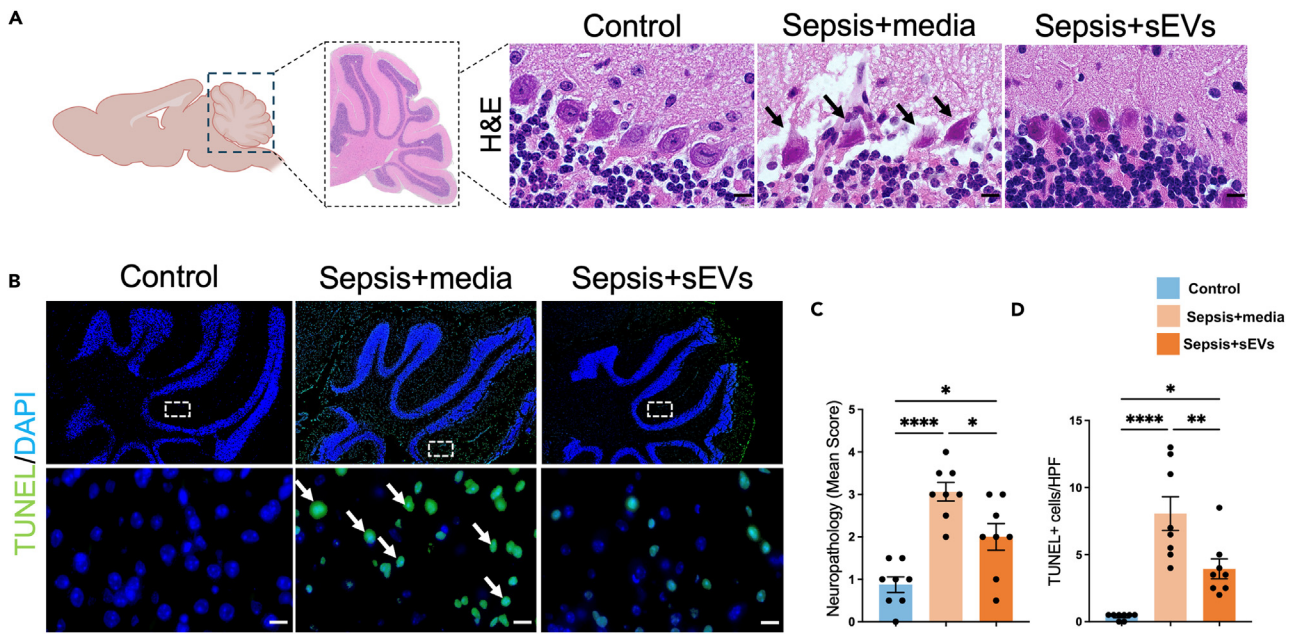

Figure 2. Sepsis-induced cerebellar injury is reversed by MSC-derived sEVs

(A–D) Representative photomicrographs of H&E and TUNEL staining in the mouse cerebellum show significant histopathological alterations during sepsis. Compared to controls, which exhibited intact cellular architecture with clear, rounded nuclei, the septic mouse cerebellum displayed (A) significant histopathological alterations including shrunken PCs, pyknotic nuclei (black arrows), perineuronal vacuole formation (Materials and Methods: Tissue processing and histological assessment) and (B) increased TUNEL labeled cells (white arrows) indicating DNA fragmentation and cell death. Overall, sepsis resulted in (C) increased neuropathological score and (D) TUNEL+ cells (****$p < 0.0001$ and ****$p < 0.0001$) which both improved with MSC-derived sEV treatment (*$p = 0.0155$ and **$p = 0.0063$). Data are represented as mean ± SEM, one-way ANOVA. Scale bar = 10 μm, Control ($n = 7$), Sepsis+media ($n = 8$), Sepsis+MSC-derived sEVs ($n = 8$). ANOVA: Analysis of Variance, DNA: Deoxyribonucleic Acid, H&E: Hematoxylin and Eosin, NS: non-significant, PC: Purkinje cells, TUNEL: Terminal deoxynucleotidyl transferase (TdT) dUTP Nick-End Labeling, MSC-derived sEV: mesenchymal stem cell-derived small extracellular vesicles.

attenuated the development of reactive astrocytosis as indicated by the decreased expression of GFAP+ in the PC and molecular layer (26.67 ± 4.82 vs. 44.17 ± 4.53, p=0.0057), (Figures S2A and S2B). Astrocytes secrete cytokines which may be neurotrophic or inflammatory depending on whether they are in a resting phase or during injury.[26] To identify the underlying mechanism of astrocytosis-induced PC damage, we aimed to define the expression of inflammatory cytokines (TNF-α)[24] and (IL-17α)[25,27] in the PC layer of the cerebellar cortex during acute sepsis. TNF-α has been shown to be a crucial mediator of neuroinflammation and SE. Its presence is associated with loss of astrocyte functions such as progressive loss of adhesion capabilities, which is dose dependent and correlates with astrocyte compromise and nuclear condensation.[28] TNF-α was expressed and co-localized with the PCs and their dendrites. TNF-α expression significantly increased in sepsis compared to controls (5.2 ± 1.1 vs. 1.4 ± 0.2, $p = 0.0085$), however, treatment with MSC-derived sEVs restored its expression to almost control levels (1.9 ± 0.2, $p = 0.03$) (Figure 5A). Notably, TNF-α was not expressed in parvalbumin (PV)+ interneurons that surround the PCs. The number of the PV + interneurons was not affected in our acute sepsis model (Figure 5C).

The expression of IL-17α was similar in control and septic mice (5.62E+09 ± 2.7E+08 vs. 7.8E+09 ± 3.7E+08, $p = 0.1096$). Treatment with MSC-derived sEVs doubled its expression (1.52E+10 ± 1.3E+09, p=<0.0001) (Figure 5B). Taken together, these findings indicate that during the acute phase of sepsis, reactive astrocytosis is a key factor for the neuronal response to injury, which is regulated by pro- and anti-inflammatory cytokines such as TNF-α and IL-17α and results in neuronal death. Treatment with MSC-derived sEVs at this phase of sepsis restores the cytokine imbalance and prevents overall neuropathological changes induced by sepsis.

MSC-derived sEVs restore basal and non-mitochondrial respiration in septic mouse cerebellum

Following observations that sepsis alters the cerebellar transcriptome, particularly in terms of energy production, and building on our findings that MSC-derived sEVs mitigate the severity of cerebellar injury as part of a hypothesized relief of immunometabolic dysfunction, we assessed the impact of MSC-derived sEVs on cerebellar energetics. To evaluate cerebellar mitochondrial function, which is directly related to energy production, we utilized the Seahorse technology (Agilent, Santa Clara, CA) to measure oxygen consumption (OCR), which is indicative of OXPHOS. Using these measurements, we determined basal respiration (cellular respiration at baseline), maximum respiration (respiration uncoupled from ATP production), and non-mitochondrial respiration in septic MSC-derived sEV-treated and untreated mice, as well as controls. In this set of experiments, we examined control mice that were given MSC-derived sEVs to investigate whether EV treatment has any

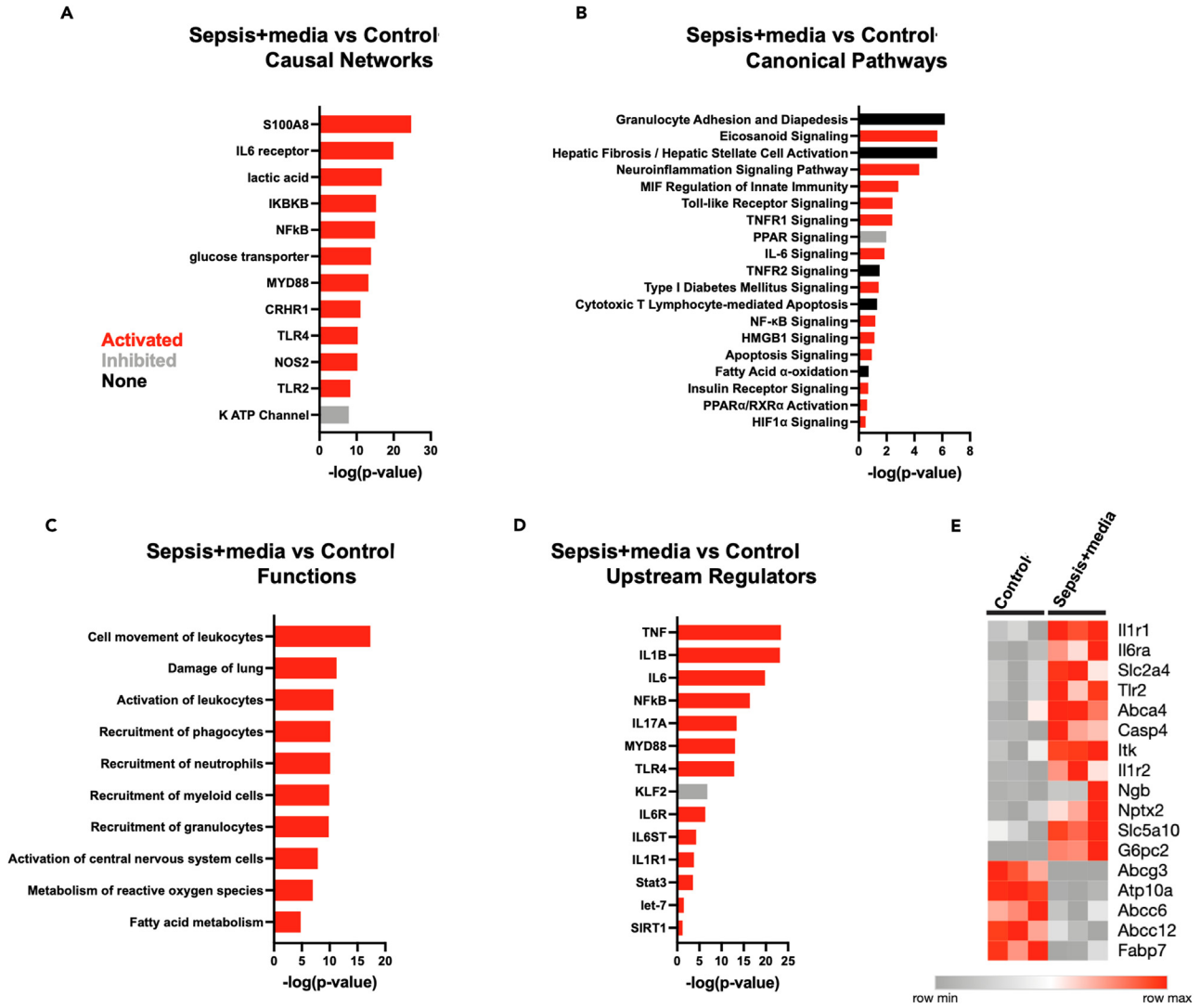

Figure 3. Sepsis induces alterations in the cerebellar transcriptome

RNA-seq reveals changes in cerebellar transcriptome following sepsis.

(A and B) Predicted activated (red) and inhibited (gray) causal networks and canonical pathways (determined by directional z-scores) in septic mice compared to controls. Ranked based on *p* value as determined using Fisher's exact test.

(C) Predicted increases (red) in cell and molecular functions (determined by directional z-scores in septic mice compared to controls. Ranked based on *p*-value as determined using Fisher's exact test.

(D) Predicted activated (red) and inhibited (gray) upstream regulators (determined by directional z-scores) in septic mice compared to controls. Ranked based on *p* value as determined using Fisher's exact test.

(E) Heatmap of most significantly predicted upstream regulators when septic mice are compared to controls. Boxes are colorized with z-scores (red = activated, gray = inactivated). Source data are provided as a Source Data file.

effect in non-septic mice. When we compared the control and control that received MSC-derived sEVs groups, we did not observe any significant changes in basal respiration, maximal respiration, non-mitochondrial OCR, and ATP-linked respiration (Figures 3A–3D). In sepsis, treatment with MSC-derived sEVs restored the basal respiration of cerebellum used to meet the endogenous ATP demand, from 236.1 ± 19.1 to 332.4 ± 40.35 ($p = 0.0337$), which was similar to controls (311.0 ± 38.2, $p = 0.3146$) (Figure 6A). The maximum respiration that the cerebellar tissue achieved with no ATP production involved was also lower under septic conditions (161.9 ± 24.0 vs. 298.7 ± 35.9 in controls that received sEV-depleted media, $p = 0.0180$). When MSC-derived sEV treatment was given, we observed an upward trend that did not reach significance ($p = 0.07$) (Figure 6B). Importantly, non-mitochondrial respiration was increased in sepsis as compared to non-septic controls that received MSC-derived sEVs [268.2 ± 36.4 vs.127.3 ± 19.3 ($p = 0.0051$)], with a normalization following MSC-derived sEV treatment (79.3 ± 8.6, $p = 0.0048$) (Figure 6C). Such an increase in non-mitochondrial respiration occurs under septic conditions via other metabolic processes such

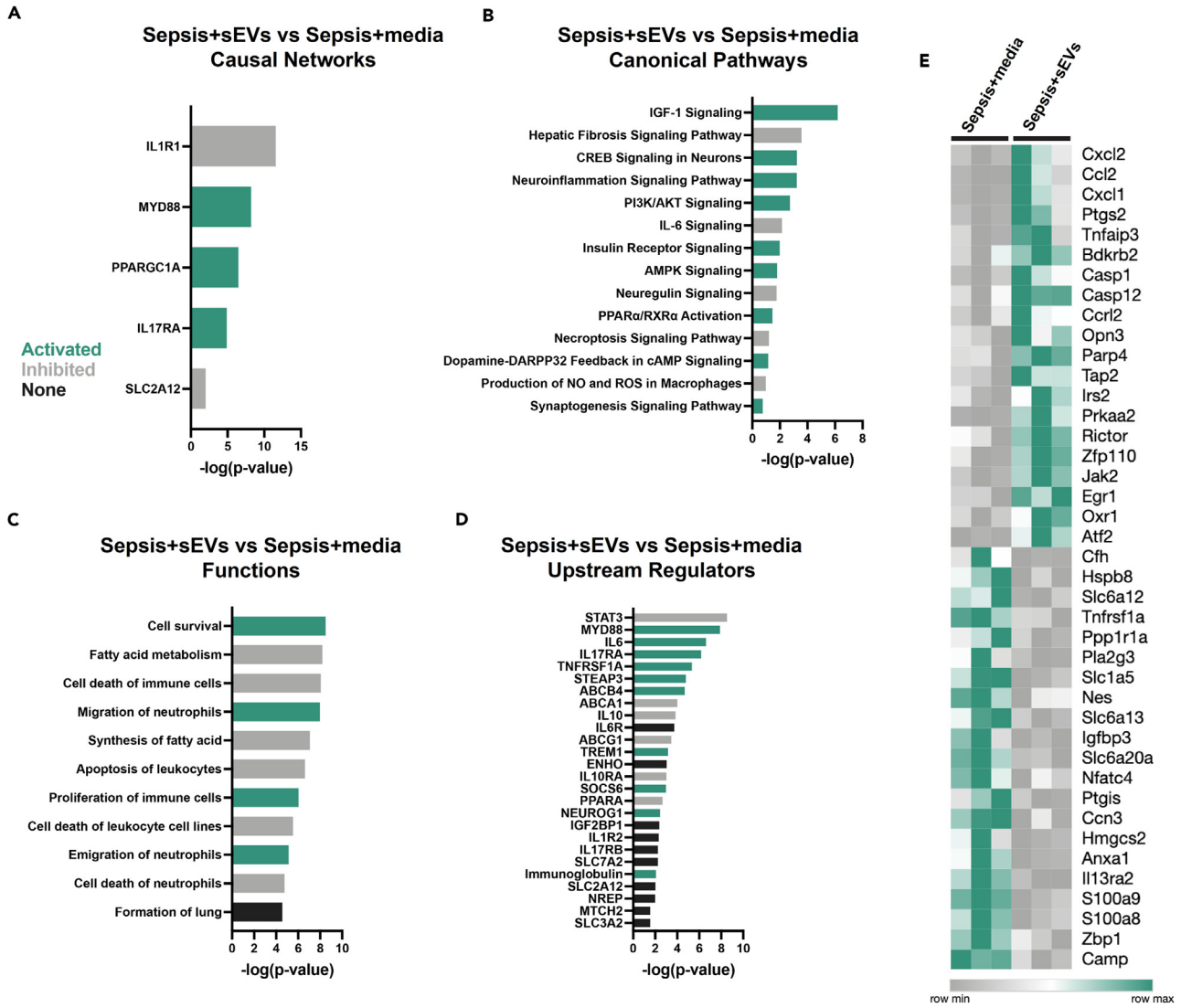

Figure 4. RNA-seq reveals MSC-derived sEV-induced changes in cerebellar transcriptome following sepsis

(A and B) Predicted activated (green) and inhibited (gray) causal networks and canonical pathways (determined by directional z-scores) in septic mice treated with MSC-derived sEVs compared to untreated septic mice. Ranked based on *p* value as determined using Fisher's exact test.

(C) Predicted increases (green) and decreases (gray) in cell and molecular functions (determined by directional z-scores) in septic mice treated with MSC-derived sEVs compared to untreated septic mice. Ranked based on *p* value as determined using Fisher's exact test.

(D) Predicted activated (green) and inhibited (gray) upstream regulators (determined by directional z-scores) in in septic mice treated with MSC-derived sEVs compared to untreated septic mice. Ranked based on *p* value as determined using Fisher's exact test.

(E) Heatmap of most significantly predicted upstream regulators when septic mice treated with MSC-derived sEVs are compared to untreated septic mice. Boxes are colorized with z-scores (green = activated, gray = inactivated). Source data are provided as a source data file.

as the pentose phosphate pathway. Lastly, ATP-linked respiration did not differ between groups despite a higher average OCR in septic mice that received MSC-derived sEV treatment likely due to the short period of time in which observations occurred (Figure 6D). These data suggest that the MSC-derived sEVs treatment can restore basal respiration in the septic cerebellum with a reduction in non-mitochondrial OCR, favoring OXPHOS.

MSC-derived sEVs alter the activation of miRNAs in the septic cerebellum

Based on our findings on the cerebellar transcriptome, we aimed to identify a potential mechanism by which MSC-derived sEVs affect the cerebellum during sepsis. First, we defined the molecular profile of the MSC-derived sEVs using miRNA sequencing (Table 2). Importantly, miRNAs, and pre-miRNA regulators whose expression was downregulated in the septic cerebellum, were upregulated in the MSC-derived

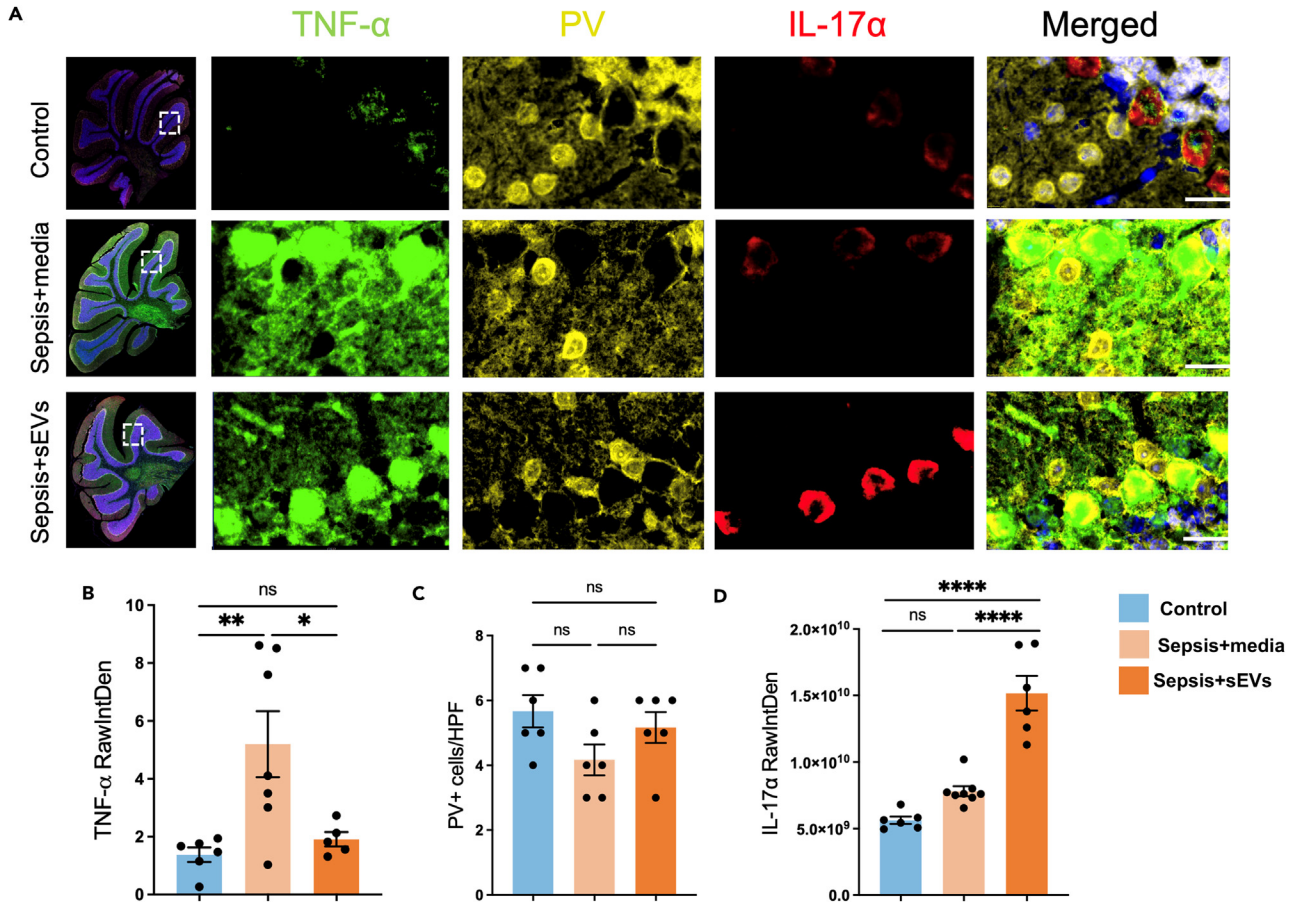

Figure 5. MSC-derived sEVs affect cytokine concentration in septic mouse cerebellum

TNF-α and IL-17α assessed by immunofluorescence.

(A) Representative photomicrograph of TNF-α, PV and IL-17α staining in low (x1.4, left) and high (×60, right) magnification of the area included in the hatched box. TNF-α was expressed and co-localized with the PC and their dendrites.

(B and C) TNF-α expression significantly increased in SE compared to controls (5.2 ± 1.1 vs. 1.4 ± 0.2, $p = 0.0085$), however, treatment with MSC-derived sEVs restored its expression by more than 50% (1.9 ± 0.2, $p = 0.03$). Notably, TNF-α was not expressed in parvalbumin (PV)+ interneurons (a and c) that surround the PCs.

(D) The expression of IL-17α was similar in control and septic mice (5.62E+09 ± 2.7E+08 vs. 7.8E+09 ± 3.7E+08, $p = 0.1096$), however, treatment with MSC-derived sEVs doubled its expression (1.52E+10 ± 1.3E+09, p=<0.0001). Data are represented as mean ± SEM, one-way ANOVA. Scale bar = 10 μm, Control ($n = 6$), Sepsis+media [for TNF-α ($n = 7$) and IL-17α ($n = 8$)], Sepsis+MSC-derived sEVs [(for TNF-α ($n = 5$) and IL-17α ($n = 6$)]. MSC-derived sEV: mesenchymal stem cell-derived small extracellular vesicles, NS: non-significant, TNFα: tumor necrosis factor alpha, IL-17α: interleukin 17 alpha, ANOVA: Analysis of Variance, PV: parvalbumin.

sEV-treated group (Figures 7A and 7B). Interestingly, many of the miRNAs that were altered in the septic cerebellum were also present in the MSC-derived sEVs (Table 2), allowing us to make associations between MSC-derived sEV cargo (miRNAs) and RNA changes in the cerebellum.

In the cerebellum of septic mice, miRNAs and pre-miRNAs of interest were inhibited (Figure 7A). This is a significant finding, since in most cases miRNAs themselves have inhibitory properties. mir-21, a precursor to miR-21 that is often overexpressed in neutrophils and macrophages in sepsis,[29] was predicted to be inhibited in the septic cerebellum. Additionally, lower miR-199a-5p levels have been correlated with poor clinical outcomes[30] and in our analysis miR-199a-5p was predicted to be inhibited in the septic cerebellum. Moreover, miR-146a-5p, which has been implicated in sepsis pathogenesis[31] was also predicted to be inhibited in the cerebellum during sepsis (Figure 7A). It is worth noting that the mature miRNAs of other pre-miRNAs, such as mir-17 and mir-181 that have been associated with improved outcomes in sepsis,[32] were also predicted to be inhibited in the untreated septic mice. Additionally, during sepsis followed by treatment with MSC-derived sEVs, some of the above miRNAs, such as miR-199a-5p as well as pre-miRNAs including mir-21, were predicted to be activated when compared to the untreated septic group (Figure 7B). Let-7-5p and miR-21-5p were the most abundant miRNAs in the MSC-derived sEVs and were predicted to be activated in the cerebellum of MSC-derived sEV-treated mice. Similarly, miR-29b-3p, miR-199a-5p, miR-30c-5p were

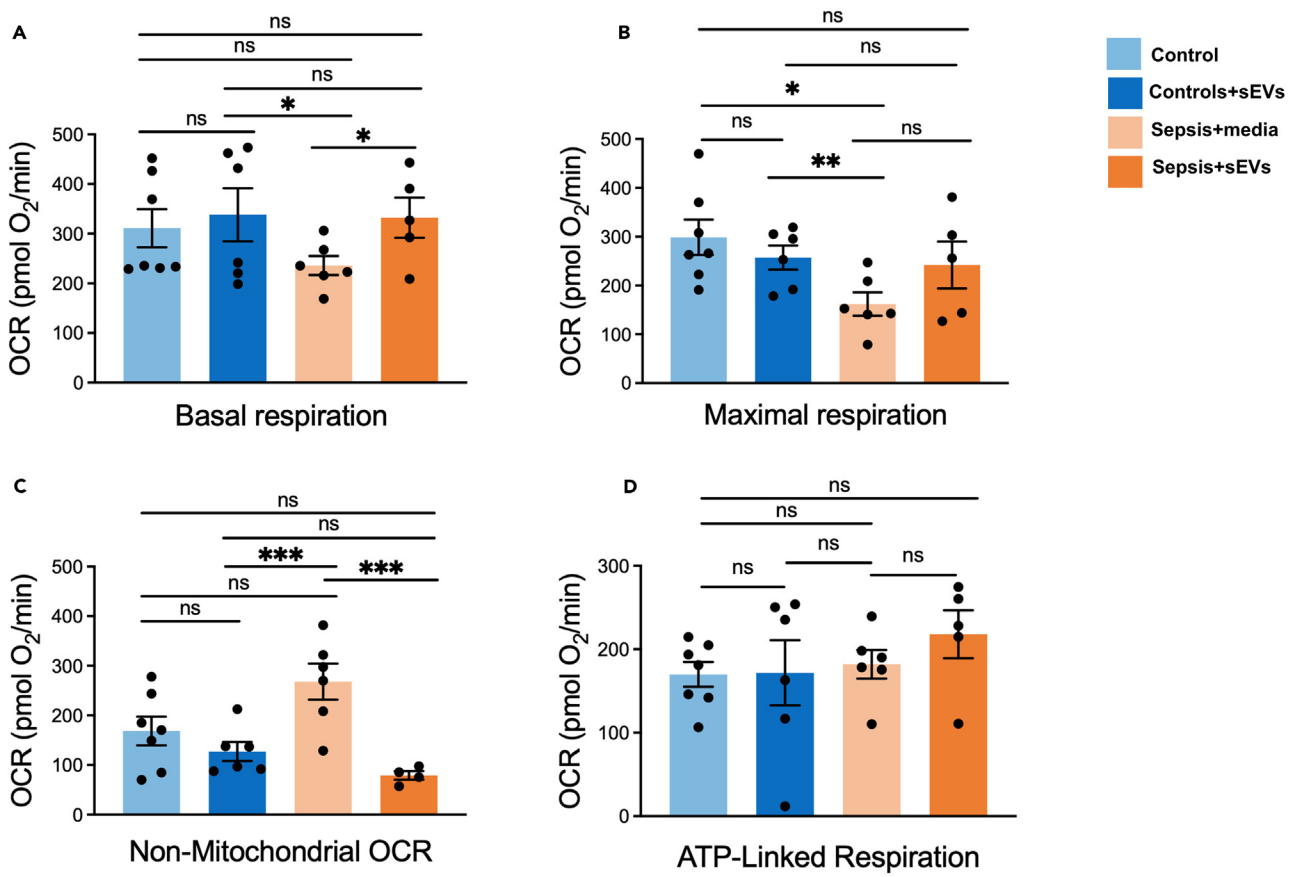

Figure 6. MSC-derived sEVs restore basal and non-mitochondrial respiration in septic mouse cerebellum

Cellular respiration measured with Seahorse technology in mice.

(A) Basal respiration decreases in sepsis [236.1 ± 19.1 vs. 311.0 ± 38.2 (*p = 0.0226)], but significantly improves with MSC-derived sEV treatment (332.4 ± 40.4, *p = 0.0337) to levels similar to controls (311.0 ± 38.2, p = 0.3146).

(B) Cerebellar tissue shows lower maximum respiration in sepsis that is trending higher with MSC-derived sEV administration but did not reach significance (p = 0.07).

(C) Non-mitochondrial respiration i.e., OCR attributable to ROS production or pentose phosphate pathway increases under septic conditions [268.2 ± 36.4 vs.127.3 ± 19.3 (***p = 0.0051)], but not with treatment (79.3 ± 8.6, ***p = 0.0048), indicating that MSC-derived sEVs favor OXPHOS-linked ATP production.

(D) Although the average ATP-linked respiration showed improvement with sEV treatment, there was no statistically significant difference among the groups, likely due to the short period of time in which observations occurred. Data are represented as mean ± SEM, one-way ANOVA. Control+media (n = 5), Control+MSC-derived sEVs (n = 5), Sepsis+media (n = 5), Sepsis+MSC-derived sEVs (n = 5). OCR: Oxygen consumption rate, ROS: reactive oxygen species, OXPHOS: oxidative phosphorylation, ATP: adenosine triphosphate, MSC-derived sEV: mesenchymal stem cell-derived small extracellular vesicles, NS: non-significant.

isolated from the MSC-derived sEVs and were also predicted to be activated in the cerebellum of septic MSC-derived sEVs-treated mice. However, miR-26a-5p and miR-155-5p were predicted to be inhibited in the cerebellum of those mice, although it was isolated in abundance in the MSC-derived sEV cargo.

DISCUSSION

Our study highlights the importance of focusing on both metabolism and innate immunity in CNS failure caused by sepsis. We examined one of the most affected CNS areas in SE, the cerebellum,[7,8] through an established murine model of sepsis.[33] We anticipated similar findings to human sepsis as the cerebellum sustained significant injury under septic conditions in postmortem examinations.[34] Moreover, the results of our study using our acute sepsis murine model have strong clinical relevance since the timeline of severe human sepsis/septic shock is similar. Mortality rates are particularly high for the first 6–24 h, especially in patients that are not recognized and treated early.[35] This model of sepsis and subsequent treatment with MSC-derived sEVs can provide valuable insight into the underlying mechanisms of SE pathophysiology and potential therapeutic interventions.

For the past decade, a new field that focuses on the interaction of innate immunity and metabolism has emerged, which has shed light on some of the possible cellular processes that lead to organ failure in sepsis.[36] A shift in cellular metabolism of glucose triggered when trained

Table 2. miRNA counts in administered MSC-derived sEV samples (sEV cargo) following miRNA sequencing

miRNA (number of copies)	Sample 1	Sample 2	Sample 3
miR-29-3p	286	197	1950
miR-199-5p	118	101	1013
miR-26-5p	1379	3375	38076
miR-30-5p	776	1092	14465
miR-21-5p	7263	14475	97957
miR-155-5p	178	604	1504
Let-7-5p	22602	39245	118496
miR-146-5p	97	1754	26544

The number of miRNA copies varies among samples, but specific miRNA presence remains consistent.

immunity is activated indicates that metabolic reprogramming is key for the observed immune response.[37] A deeper understanding of the complex relationship between metabolism and the immune system can help us develop treatments that will rely on the metabolic manipulation of immune cells with the goal to alleviate the imbalance between hyperimmune response and immune paralysis observed in sepsis. The concept of immunometabolism, however, has yet to receive much focus in the context of CNS infectious processes. Some studies support the hypothesis that metabolism is the driver of microglia function and macrophage phenotype in acute and chronic inflammatory conditions, such as Alzheimer's disease, stroke, or traumatic brain injury (TBI).[38] In sepsis, mixed pro-inflammatory and anti-inflammatory macrophage phenotypes are dependent on the balance between energy-generating pathways.[39] Pro-inflammatory states require fast glucose utilization for ATP production via glycolysis whereas reparative states rely on energy efficient OXPHOS.[40] In this study, we evaluate the role of the complex interplay between metabolic and immunologic pathways in the pathophysiology of sepsis and more specifically, SE.

Energy deficit is a crucial factor in SE pathophysiology. It is well known that OXPHOS is the energetic pathway that powers presynaptic and postsynaptic mechanisms responsible for brain information processing.[28] Similar to other pre-clinical studies, we demonstrated that in infection, mitochondrial dysfunction, as evident by OXPHOS impairment, leads to decreased overall ATP.

In this study, MSC-derived sEV administration led to an increase in basal respiration necessary to meet cellular energetic demands, and at the same time, shifted the cells back to the more energy efficient OXPHOS. Although we did not observe an overall ATP production change, the significant rise in non-mitochondrial OCR in sepsis implied a suppressed aerobic metabolism and it was indicative of poor oxygen consumption. Oxygen is then diverted to enzymatic ROS production or to other non-ATP producing pathways, such as the pentose phosphate pathway. These changes in cellular respiration and metabolic profile correlated well with an improvement in immune dysregulation, toward a more balanced inflammatory response as assessed by cerebellar tissue cytokine examination production.[40–44] Although previous reports identified MSCs as a potential therapy for an improved energetic profile,[18,45] we demonstrated that MSC-derived sEVs alone have comparable properties because of their cargo (miRNA and proteins[18]) that targets specific metabolic pathways.

In our murine sepsis model, in agreement with previous reports on clinical and pre-clinical studies, the cerebellar cortex displayed significant neuropathology under acute septic conditions, which was then reversed by MSC-derived sEV treatment.[7,8,41,42,46] Cytokine concentrations were also altered in the septic cerebellum compared to controls. TNF-α, a key mediator of inflammation in sepsis,[43] was prominent in septic samples, indicating an imbalance in neuro-immune response. MSC-derived sEV administration led to a normalization of TNF-α concentration, a finding consistent with current research.[44] Importantly, IL-17α, a cytokine which contributes to host protection against infectious organisms,[25] was not elevated in the septic cerebellum but was induced by MSC-derived sEVs. IL-17α also participates in the remodeling of the CNS and ameliorates the expression of social behavior deficits in mice,[27] properties that can explain some of the neuroprotective effects of sEVs in SE. It is also possible that sEVs carry specific cytokines[47] that actively regulate the immune response in SE.

As expected, in the septic cerebellar transcriptome, immune pathways were predicted to be activated with regulators, including inflammatory cytokines such as IL-1, IL-6 and TNF-α. Immune cell proliferation, activation, and migration correspond to a hyperimmune response that is present at least during the initial phase of sepsis.[48] It is possible that the observed clinical improvement in MSC-derived sEV-treated septic mice is secondary to the beneficial effects of MSC-derived sEVs on systemic inflammation, not only in the cerebellum. Increased metabolic demand under septic conditions corresponded to predicted activated fatty acid metabolism. Additionally, apoptotic mechanisms in SE were also predicted to be upregulated, likely explaining the observed neuropathological changes. Many of the same immunologic pathways were predicted to be altered when MSC-derived sEVs were administered. IL-6 signaling was downregulated, although the neuroinflammation signaling and IL-17 receptor regulators were not, suggesting an ongoing but more balanced inflammatory response that is necessary during an infectious disease. Interestingly, metabolic pathways, including those involving the PPARs as well as pathways that promote synaptogenesis and neuroprotection through neurotrophins and anti-apoptotic genes, were found to be activated after MSC-derived sEV treatment, highlighting a favorable profile of MSC-derived sEVs as therapeutic agents in SE. Our analyses into the impact of sepsis on cerebellar gene expression unveils extensive alterations, including the upregulation of immune and inflammatory pathways and shifts in metabolic functions. This study highlights the potential of MSC-derived sEVs to modulate these sepsis-induced changes. This not only suggests a

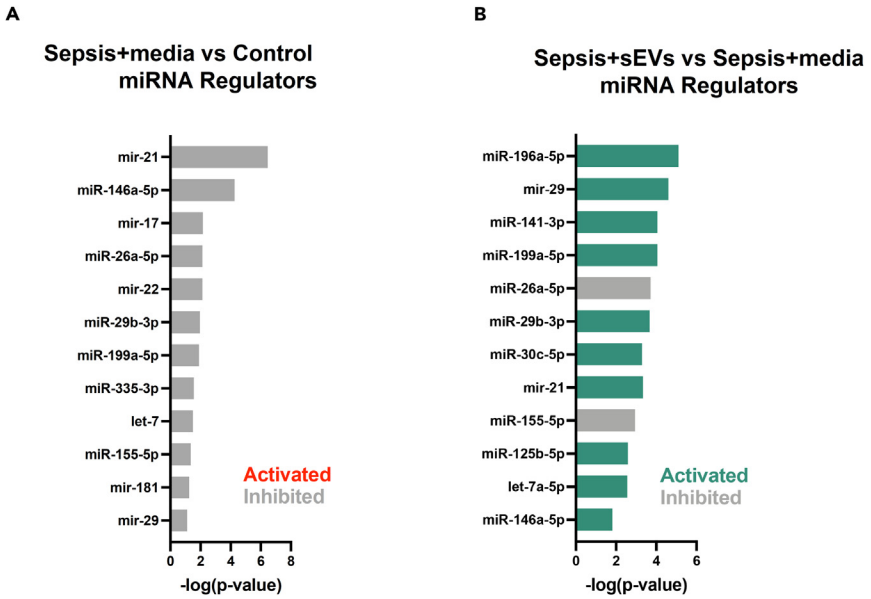

Figure 7. MSC-derived sEVs alter the activation of miRNAs in the septic cerebellum

(A) Predicted inhibited (gray) miRNAs (determined by directional z-scores) in septic mice compared to controls. Ranked based on *p* value as determined using Fisher's exact test. Most miRNAs of interest are inhibited, indicating that they do not have any predicted inhibitory effects on their target mRNA.

(B) Predicted activated (green) and inhibited (gray) miRNAs (determined by directional z-scores) in septic MSC-derived sEV-treated mice compared to untreated septic mice. Ranked based on *p* value as determined using Fisher's exact test. Several miRNAs inhibited in septic mice that received sEV-depleted media were predicted to be activated in the septic mice that received MSC-derived sEVs. Source data are provided as a source d file.

therapeutic avenue for reducing inflammation but also for supporting cerebellar function by adjusting metabolic and immune responses, indicating a nuanced strategy to counteract the cerebellar effects of sepsis.

MSC-derived sEVs mainly carry miRNAs and proteins,[49] which can suggest that miRNAs are at least partially responsible for their effects. Specific miRNAs isolated from our MSC-derived sEVs that have been shown in studies to be involved in improved outcomes in sepsis,[29,30] were also predicted to be activated in the cerebellum of MSC-derived sEV-treated mice compared to untreated mice. For example, miR-21 is overexpressed in neutrophils and macrophages in sepsis[29] and miR-146a-5p and miR-199a induce TNF-α and IL-6 production and a strong innate immune response.[30,50] Downregulation of those miRNAs induces attenuation of sepsis-related organ injury.[30] It was recently reported that miR-30, Let-7, miR-15, miR-26 and miR-338 directly control mitochondrial dynamics and OXPHOS and that miR-30c-5p alters metabolic pathways to maintain the homeostasis of lipid metabolism.[16,51–55] In this work, we demonstrated that members of the let7, mir21 and mir30 families including mir-30c-5p are present in abundance in MSC-derived sEVs and were also activated in the MSC-derived sEV-treated septic cerebellum, pointing to the important regulatory role and therapeutic potential of the sEV cargo (Figure 7B). In most cases, activated miRNAs inhibit their target mRNA, altering gene expression and cellular processes. It becomes apparent that those miRNAs can also be therapeutic targets within engineered sEVs. The potential of MSC-derived sEVs and their carried miRNAs as potential treatments have also been described in cancer where immune response and metabolic demands can be similar to sepsis.[56–58] It is therefore imperative to design more preclinical studies with MSC-derived sEVs and identify miRNAs as treatment modalities in multi-organ failure in sepsis.

In conclusion, this is the first study to show a potential direct effect of MSC-derived sEVs in an SE murine model. We showed that the cerebellum is a major brain region to sustain significant injury in sepsis, which is in line with previous reports that highlight the vulnerability of the cerebellum to infectious processes.[7,8,41,42,46] We demonstrated that in SE, MSC-derived sEVs can alter cell respiration of neural cells *in vivo*, leading to improved metabolism and a balanced cerebellar inflammatory response. MSC-derived sEVs present an opportunity for the development of new therapeutic protocols for SE and other conditions that cause brain injury. Sepsis is a heterogeneous disease that can cause multi-organ dysfunction and we can determine based on our results that energy deficiency and immune dysregulation play an important role in this disease pathophysiology. This work sheds light on the immunometabolic changes that take place in SE that have implications for short- and long-term CNS dysfunction. A reversal of those changes can lead to favorable clinical outcomes and MSC-derived sEVs seem to be a viable therapeutic option for SE, that is potentially translatable to humans. Building upon our promising findings, we propose several research directions to further explore the therapeutic potential of MSC-derived sEVs in treating SE. Firstly, delving deeper into the specific miRNAs identified in our study and investigating their individual roles could illuminate the mechanisms through which these sEVs exert their beneficial effects. Moreover, the development of engineered sEVs, enriched with these specific miRNAs identified as beneficial, could offer a tailored therapeutic approach. Lastly, expanding our focus to investigate alternative sEV cargo,

such as proteins, could uncover additional therapeutic targets or biomarkers, further broadening our understanding of the sEV mechanism in SE treatment. These directions not only pave the way for comprehensive mechanistic insights, but also underscore the innovative potential of MSC-derived sEVs in SE therapy.

Limitations of the study

We recognize that there are limitations to our approach. Although our murine model of sepsis closely resembles the pathophysiology of human acute infection, there are differences that require the design of clinical trials to study our treatment in humans. Additionally, in clinical practice, sepsis management consists of antibiotics and intravenous fluids that we did not administer in our model due to the heterogeneity in treatment response (for both antibiotics and intravenous fluids) that would not allow us to have an accurate assessment of the exact role of MSC-derived sEVs as therapeutic agents.[59] Furthermore, although we describe the potential mechanism by which MSC-derived sEVs exhibit their therapeutic effects (miRNAs), there is potentially other sEV cargo, such as proteins, that can alter immune and metabolic pathways. Although not explicitly detected, we are confident the MSC-derived sEVs reached the CNS based on multiple reports[22] and the changes we identified in the histological analyses of brain samples. Finally, there is a possibility that MSC-derived sEVs have a direct effect on bacteria, which was not accounted for in our study. If proven, this would also enhance the significant therapeutic role of MSC-derived sEVs in sepsis and SE.

STAR★METHODS

Detailed methods are provided in the online version of this paper and include the following:

- KEY RESOURCES TABLE
- RESOURCE AVAILABILITY
  - Lead contact
  - Materials availability
  - Data and code availability
- EXPERIMENTAL MODEL AND STUDY PARTICIPANT DETAILS
- METHOD DETAILS
  - Murine model of sepsis
  - Isolation and characterization MSC-derived sEVs
  - Tissue processing and histological assessment
  - Image acquisition and analysis
  - OXPHOS assessment by seahorse in cerebellar samples
  - Cerebellar tissue RNA sequencing
  - MSC-derived sEV miRNA sequencing
- QUANTIFICATION AND STATISTICAL ANALYSIS

SUPPLEMENTAL INFORMATION

Supplemental information can be found online at https://doi.org/10.1016/j.isci.2024.110573.

ACKNOWLEDGMENTS

Dr. John Gaughan from Temple University (Philadelphia, PA) assisted in the statistical analysis.

Dr. John W. Ludlow from Zen-Bio Inc. provided us with electron microscopy images and protein characterization of MSC-derived sEVs. This work was supported by a NICHD K12HD001399 award (I.K.), NICHD K12HD001399 award (P.K.), NINDS Javits award R37NS109478 (V.G.) and NICHD P50HD105328 award (V.G.).

AUTHOR CONTRIBUTIONS

I.K. conceived the current study, performed all experiments, and authored the manuscript. P.K. performed histopathologic and seahorse experiments and analyses and co-authored the manuscript. C.H., E.G., J.B., and W.O. assisted in all experiments and RNA-seq analysis and edited the manuscript. G.S., C.B., and M.T. edited the manuscript and made the necessary revisions. R.F. and V.G. oversaw this project and provided feedback at all stages of the experimental work including the interpretation of results and manuscript preparation. All authors read and approved the manuscript.

DECLARATION OF INTERESTS

The authors declare that they have no conflict of interest.

Received: December 21, 2023
Revised: May 20, 2024
Accepted: July 22, 2024
Published: July 25, 2024

REFERENCES

1. Rudd, K.E., Johnson, S.C., Agesa, K.M., Shackelford, K.A., Tsoi, D., Kievlan, D.R., Colombara, D.V., Ikuta, K.S., Kissoon, N., Finfer, S., et al. (2020). Global, regional, and national sepsis incidence and mortality, 1990-2017: analysis for the Global Burden of Disease Study. Lancet *395*, 200–211. https://doi.org/10.1016/s0140-6736(19)32989-7.
2. van der Poll, T., Shankar-Hari, M., and Wiersinga, W.J. (2021). The immunology of sepsis. Immunity *54*, 2450–2464. https://doi.org/10.1016/j.immuni.2021.10.012.
3. Gyawali, B., Ramakrishna, K., and Dhamoon, A.S. (2019). Sepsis: The evolution in definition, pathophysiology, and management. SAGE Open Med. *7*, 2050312119835043. https://doi.org/10.1177/2050312119835043.
4. Zhao, Q., Ren, H., Feng, S., Chi, Y., He, Y., Yang, D., Ma, F., Li, J., Lu, S., Chen, F., et al. (2015). Aberrant expression and significance of OCT-4A transcription factor in leukemia cells. Blood Cells Mol. Dis. *54*, 90–96. https://doi.org/10.1016/j.bcmd.2014.07.014.
5. Feigenson, M., Eliseev, R.A., Jonason, J.H., Mills, B.N., and O'Keefe, R.J. (2017). PGE2 Receptor Subtype 1 (EP1) Regulates Mesenchymal Stromal Cell Osteogenic Differentiation by Modulating Cellular Energy Metabolism. J. Cell. Biochem. *118*, 4383–4393. https://doi.org/10.1002/jcb.26092.
6. Fujishima, S., Gando, S., Saitoh, D., Kushimoto, S., Ogura, H., Abe, T., Shiraishi, A., Mayumi, T., Sasaki, J., Kotani, J., et al. (2020). Demographics, Treatments, and Outcomes of Acute Respiratory Distress Syndrome: the Focused Outcomes Research in Emergency Care in Acute Respiratory Distress Syndrome, Sepsis, and Trauma (FORECAST) Study. Shock *53*, 544–549. https://doi.org/10.1097/SHK.0000000000001416.
7. Aslankoc, R., Savran, M., Ozmen, O., and Asci, S. (2018). Hippocampus and cerebellum damage in sepsis induced by lipopolysaccharide in aged rats - Pregabalin can prevent damage. Biomed. Pharmacother. *108*, 1384–1392. https://doi.org/10.1016/j.biopha.2018.09.162.
8. Savran, M., Aslankoc, R., Ozmen, O., Erzurumlu, Y., Savas, H.B., Temel, E.N., Kosar, P.A., and Boztepe, S. (2020). Agomelatine could prevent brain and cerebellum injury against LPS-induced neuroinflammation in rats. Cytokine *127*, 154957. https://doi.org/10.1016/j.cyto.2019.154957.
9. Harbeson, D., Francis, F., Bao, W., Amenyogbe, N.A., and Kollmann, T.R. (2018). Energy Demands of Early Life Drive a Disease Tolerant Phenotype and Dictate Outcome in Neonatal Bacterial Sepsis. Front. Immunol. *9*, 1918. https://doi.org/10.3389/fimmu.2018.01918.
10. Uehara, M., Plank, L.D., and Hill, G.L. (1999). Components of energy expenditure in patients with severe sepsis and major trauma: a basis for clinical care. Crit. Care Med. *27*, 1295–1302. https://doi.org/10.1097/00003246-199907000-00015.
11. Occhiali, E., Urli, M., Pressat-Laffouilhere, T., Achamrah, N., Veber, B., and Clavier, T. (2021). Dynamic metabolic changes measured by indirect calorimetry during the early phase of septic shock: a prospective observational pilot study. Eur. J. Clin. Nutr. *76*, 693–697. https://doi.org/10.1038/s41430-021-01012-2.
12. Hirasawa, H., Oda, S., and Nakamura, M. (2009). Blood glucose control in patients with severe sepsis and septic shock. World J. Gastroenterol. *15*, 4132–4136. https://doi.org/10.3748/wjg.15.4132.
13. Singer, M. (2016). The new sepsis consensus definitions (Sepsis-3): the good, the not-so-bad, and the actually-quite-pretty. Intensive Care Med. *42*, 2027–2029. https://doi.org/10.1007/s00134-016-4600-4.
14. Gofton, T.E., and Young, G.B. (2012). Sepsis-associated encephalopathy. Nat. Rev. Neurol. *8*, 557–566. https://doi.org/10.1038/nrneurol.2012.183.
15. Morrison, T.J., Jackson, M.V., Cunningham, E.K., Kissenpfennig, A., McAuley, D.F., O'Kane, C.M., and Krasnodembskaya, A.D. (2017). Mesenchymal Stromal Cells Modulate Macrophages in Clinically Relevant Lung Injury Models by Extracellular Vesicle Mitochondrial Transfer. Am. J. Respir. Crit. Care Med. *196*, 1275–1286. https://doi.org/10.1164/rccm.201701-0170OC.
16. Li, P., Jiao, J., Gao, G., and Prabhakar, B.S. (2012). Control of mitochondrial activity by miRNAs. J. Cell. Biochem. *113*, 1104–1110. https://doi.org/10.1002/jcb.24004.
17. Jackson, M.V., Morrison, T.J., Doherty, D.F., McAuley, D.F., Matthay, M.A., Kissenpfennig, A., O'Kane, C.M., and Krasnodembskaya, A.D. (2016). Mitochondrial Transfer via Tunneling Nanotubes is an Important Mechanism by Which Mesenchymal Stem Cells Enhance Macrophage Phagocytosis in the In Vitro and In Vivo Models of ARDS. Stem Cell. *34*, 2210–2223. https://doi.org/10.1002/stem.2372.
18. Matthay, M.A. (2017). Extracellular Vesicle Transfer from Mesenchymal Stromal Cells Modulates Macrophage Function in Acute Lung Injury. Basic Science and Clinical Implications. Am. J. Respir. Crit. Care Med. *196*, 1234–1236. https://doi.org/10.1164/rccm.201706-1122ED.
19. Gotts, J.E., and Matthay, M.A. (2018). Cell-based Therapy in Sepsis. A Step Closer. Am. J. Respir. Crit. Care Med. *197*, 280–281. https://doi.org/10.1164/rccm.201710-2068ED.
20. Jakubec, M., Maple-Grødem, J., Akbari, S., Nesse, S., Halskau, Ø., and Mork-Jansson, A.E. (2020). Plasma-derived exosome-like vesicles are enriched in lyso-phospholipids and pass the blood-brain barrier. PLoS One *15*, e0232442. https://doi.org/10.1371/journal.pone.0232442.
21. Shrum, B., Anantha, R.V., Xu, S.X., Donnelly, M., Haeryfar, S.M.M., McCormick, J.K., and Mele, T. (2014). A robust scoring system to evaluate sepsis severity in an animal model. BMC Res. Notes *7*, 233. https://doi.org/10.1186/1756-0500-7-233.
22. Banks, W.A., Sharma, P., Bullock, K.M., Hansen, K.M., Ludwig, N., and Whiteside, T.L. (2020). Transport of Extracellular Vesicles across the Blood-Brain Barrier: Brain Pharmacokinetics and Effects of Inflammation. Int. J. Mol. Sci. *21*, 4407. https://doi.org/10.3390/ijms21124407.
23. Love, M.I., Huber, W., and Anders, S. (2014). Moderated estimation of fold change and dispersion for RNA-seq data with DESeq2. Genome Biol. *15*, 550. https://doi.org/10.1186/s13059-014-0550-8.
24. Meeuwsen, S., Persoon-Deen, C., Bsibsi, M., Ravid, R., and van Noort, J.M. (2003). Cytokine, chemokine and growth factor gene profiling of cultured human astrocytes after exposure to proinflammatory stimuli. Glia *43*, 243–253. https://doi.org/10.1002/glia.10259.
25. Ge, Y., Huang, M., and Yao, Y.M. (2020). Biology of Interleukin-17 and Its Pathophysiological Significance in Sepsis. Front. Immunol. *11*, 1558. https://doi.org/10.3389/fimmu.2020.01558.
26. Bernaus, A., Blanco, S., and Sevilla, A. (2020). Glia Crosstalk in Neuroinflammatory Diseases. Front. Cell. Neurosci. *14*, 209. https://doi.org/10.3389/fncel.2020.00209.
27. Reed, M.D., Yim, Y.S., Wimmer, R.D., Kim, H., Ryu, C., Welch, G.M., Andina, M., King, H.O., Waisman, A., Halassa, M.M., et al. (2020). IL-17a promotes sociability in mouse models of neurodevelopmental disorders. Nature *577*, 249–253. https://doi.org/10.1038/s41586-019-1843-6.
28. van Kralingen, C., Kho, D.T., Costa, J., Angel, C.E., and Graham, E.S. (2013). Exposure to inflammatory cytokines IL-1beta and TNFalpha induces compromise and death of astrocytes; implications for chronic neuroinflammation. PLoS One *8*, e84269. https://doi.org/10.1371/journal.pone.0084269.
29. De Melo, P., Pineros Alvarez, A.R., Ye, X., Blackman, A., Alves-Filho, J.C., Medeiros, A.I., Rathmell, J., Pua, H., and Serezani, C.H. (2021). Macrophage-Derived MicroRNA-21 Drives Overwhelming Glycolytic and Inflammatory Response during Sepsis via Repression of the PGE2/IL-10 Axis. J. Immunol. *207*, 902–912. https://doi.org/10.4049/jimmunol.2001251.
30. Liu, Y., Guan, H., Zhang, J.L., Zheng, Z., Wang, H.T., Tao, K., Han, S.C., Su, L.L., and Hu, D. (2018). Acute downregulation of miR-199a attenuates sepsis-induced acute lung injury by targeting SIRT1. Am. J. Physiol. Cell Physiol. *314*, C449–C455. https://doi.org/10.1152/ajpcell.00173.2017.
31. Xu, J., Feng, Y., Jeyaram, A., Jay, S.M., Zou, L., and Chao, W. (2018). Circulating Plasma Extracellular Vesicles from Septic Mice Induce Inflammation via MicroRNA- and TLR7-Dependent Mechanisms. J. Immunol. *201*, 3392–3400. https://doi.org/10.4049/jimmunol.1801008.

32. Essandoh, K., and Fan, G.C. (2014). Role of extracellular and intracellular microRNAs in sepsis. Biochim. Biophys. Acta *1842*, 2155–2162. https://doi.org/10.1016/j.bbadis.2014.07.021.
33. Lewis, A.J., Seymour, C.W., and Rosengart, M.R. (2016). Current Murine Models of Sepsis. Surg. Infect. *17*, 385–393. https://doi.org/10.1089/sur.2016.021.
34. Lucas, S. (2007). The autopsy pathology of sepsis-related death. Curr. Diagn. Pathol. *13*, 375–388. https://doi.org/10.1016/j.cdip.2007.06.001.
35. Weinberger, J., Rhee, C., and Klompas, M. (2020). A Critical Analysis of the Literature on Time-to-Antibiotics in Suspected Sepsis. J. Infect. Dis. *222*, S110–S118. https://doi.org/10.1093/infdis/jiaa146.
36. Koutroulis, I., Batabyal, R., McNamara, B., Ledda, M., Hoptay, C., and Freishtat, R.J. (2019). Sepsis Immunometabolism: From Defining Sepsis to Understanding How Energy Production Affects Immune Response. Crit. Care Explor. *1*, e0061. https://doi.org/10.1097/cce.0000000000000061.
37. Cheng, S.C., Quintin, J., Cramer, R.A., Shepardson, K.M., Saeed, S., Kumar, V., Giamarellos-Bourboulis, E.J., Martens, J.H.A., Rao, N.A., Aghajanirefah, A., et al. (2014). mTOR- and HIF-1alpha-mediated aerobic glycolysis as metabolic basis for trained immunity. Science *345*, 1250684. https://doi.org/10.1126/science.1250684.
38. Devanney, N.A., Stewart, A.N., and Gensel, J.C. (2020). Microglia and macrophage metabolism in CNS injury and disease: The role of immunometabolism in neurodegeneration and neurotrauma. Exp. Neurol. *329*, 113310. https://doi.org/10.1016/j.expneurol.2020.113310.
39. Viola, A., Munari, F., Sánchez-Rodríguez, R., Scolaro, T., and Castegna, A. (2019). The Metabolic Signature of Macrophage Responses. Front. Immunol. *10*, 1462. https://doi.org/10.3389/fimmu.2019.01462.
40. Lauro, C., and Limatola, C. (2020). Metabolic Reprograming of Microglia in the Regulation of the Innate Inflammatory Response. Front. Immunol. *11*, 493. https://doi.org/10.3389/fimmu.2020.00493.
41. Basinger, J.M., Fiester, S.E., and Fulcher, J.W. (2019). Mortality from neonatal herpes simplex viremia causing severe hepatitis. Forensic Sci. Med. Pathol. *15*, 663–666. https://doi.org/10.1007/s12024-019-00147-w.
42. Chaudhry, N., and Duggal, A.K. (2014). Sepsis Associated Encephalopathy. Adv. Met. Med. *2014*, 762320. https://doi.org/10.1155/2014/762320.
43. Spooner, C.E., Markowitz, N.P., and Saravolatz, L.D. (1992). The role of tumor necrosis factor in sepsis. Clin. Immunol. Immunopathol. *62*, S11–S17. https://doi.org/10.1016/0090-1229(92)90036-n.
44. Wu, J., Wang, Y., and Li, L. (2017). Functional significance of exosomes applied in sepsis: A novel approach to therapy. Biochim. Biophys. Acta, Mol. Basis Dis. *1863*, 292–297. https://doi.org/10.1016/j.bbadis.2016.10.024.
45. Matthay, M.A., Pati, S., and Lee, J.W. (2017). Concise Review: Mesenchymal Stem (Stromal) Cells: Biology and Preclinical Evidence for Therapeutic Potential for Organ Dysfunction Following Trauma or Sepsis. Stem Cell. *35*, 316–324. https://doi.org/10.1002/stem.2551.
46. Westhoff, D., Engelen-Lee, J.Y., Hoogland, I.C.M., Aronica, E.M.A., van Westerloo, D.J., van de Beek, D., and van Gool, W.A. (2019). Systemic infection and microglia activation: a prospective postmortem study in sepsis patients. Immun. Ageing *16*, 18. https://doi.org/10.1186/s12979-019-0158-7.
47. Murao, A., Brenner, M., Aziz, M., and Wang, P. (2020). Exosomes in Sepsis. Front. Immunol. *11*, 2140. https://doi.org/10.3389/fimmu.2020.02140.
48. Delano, M.J., and Ward, P.A. (2016). The immune system's role in sepsis progression, resolution, and long-term outcome. Immunol. Rev. *274*, 330–353. https://doi.org/10.1111/imr.12499.
49. Chen, Q.Y., Wen, T., Wu, P., Jia, R., Zhang, R., and Dang, J. (2021). Exosomal Proteins and miRNAs as Mediators of Amyotrophic Lateral Sclerosis. Front. Cell Dev. Biol. *9*, 718803. https://doi.org/10.3389/fcell.2021.718803.
50. Wang, S., Yang, Y., Suen, A., Zhu, J., Williams, B., Hu, J., Chen, F., Kozar, R., Shen, S., Li, Z., et al. (2021). Role of extracellular microRNA-146a-5p in host innate immunity and bacterial sepsis. iScience *24*, 103441. https://doi.org/10.1016/j.isci.2021.103441.
51. Li, J., Donath, S., Li, Y., Qin, D., Prabhakar, B.S., and Li, P. (2010). miR-30 regulates mitochondrial fission through targeting p53 and the dynamin-related protein-1 pathway. PLoS Genet. *6*, e1000795. https://doi.org/10.1371/journal.pgen.1000795.
52. Jiang, S. (2019). A Regulator of Metabolic Reprogramming: MicroRNA Let-7. Transl. Oncol. *12*, 1005–1013. https://doi.org/10.1016/j.tranon.2019.04.013.
53. Ricquier, D. (2005). Respiration uncoupling and metabolism in the control of energy expenditure. Proc. Nutr. Soc. *64*, 47–52. https://doi.org/10.1079/pns2004408.
54. Karbiener, M., Pisani, D.F., Frontini, A., Oberreiter, L.M., Lang, E., Vegiopoulos, A., Mössenböck, K., Bernhardt, G.A., Mayr, T., Hildner, F., et al. (2014). MicroRNA-26 family is required for human adipogenesis and drives characteristics of brown adipocytes. Stem Cell. *32*, 1578–1590. https://doi.org/10.1002/stem.1603.
55. Christian, P., and Su, Q. (2014). MicroRNA regulation of mitochondrial and ER stress signaling pathways: implications for lipoprotein metabolism in metabolic syndrome. Am. J. Physiol. Endocrinol. Metab. *307*, E729–E737. https://doi.org/10.1152/ajpendo.00194.2014.
56. Giovannetti, E., Funel, N., Peters, G.J., Del Chiaro, M., Erozenci, L.A., Vasile, E., Leon, L.G., Pollina, L.E., Groen, A., Falcone, A., et al. (2010). MicroRNA-21 in pancreatic cancer: correlation with clinical outcome and pharmacologic aspects underlying its role in the modulation of gemcitabine activity. Cancer Res. *70*, 4528–4538. https://doi.org/10.1158/0008-5472.Can-09-4467.
57. Michael, I.P., Saghafinia, S., and Hanahan, D. (2019). A set of microRNAs coordinately controls tumorigenesis, invasion, and metastasis. Proc. Natl. Acad. Sci. USA *116*, 24184–24195. https://doi.org/10.1073/pnas.1913307116.
58. Guz, M., Rivero-Müller, A., Okoń, E., Stenzel-Bembenek, A., Polberg, K., Słomka, M., and Stepulak, A. (2014). MicroRNAs-role in lung cancer. Dis. Markers *2014*, 218169. https://doi.org/10.1155/2014/218169.
59. Fohner, A.E., Greene, J.D., Lawson, B.L., Chen, J.H., Kipnis, P., Escobar, G.J., and Liu, V.X. (2019). Assessing clinical heterogeneity in sepsis through treatment patterns and machine learning. J. Am. Med. Inform. Assoc. *26*, 1466–1477. https://doi.org/10.1093/jamia/ocz106.
60. Kratimenos, P., Koutroulis, I., Agarwal, B., Theocharis, S., and Delivoria-Papadopoulos, M. (2017). Effect of Src Kinase inhibition on Cytochrome c, Smac/DIABLO and Apoptosis Inducing Factor (AIF) Following Cerebral Hypoxia-Ischemia in Newborn Piglets. Sci. Rep. *7*, 16664. https://doi.org/10.1038/s41598-017-16983-1.
61. Hoque, N., Sabir, H., Maes, E., Bishop, S., and Thoresen, M. (2014). Validation of a neuropathology score using quantitative methods to evaluate brain injury in a pig model of hypoxia ischaemia. J. Neurosci. Methods *230*, 30–36. https://doi.org/10.1016/j.jneumeth.2014.04.005.
62. Lein, E.S., Hawrylycz, M.J., Ao, N., Ayres, M., Bensinger, A., Bernard, A., Boe, A.F., Boguski, M.S., Brockway, K.S., Byrnes, E.J., et al. (2007). Genome-wide atlas of gene expression in the adult mouse brain. Nature *445*, 168–176. https://doi.org/10.1038/nature05453.
63. Franklin, K.B.J., and Paxinos, G. (2013). Paxinos and Franklin's the Mouse Brain in Stereotaxic Coordinates, Fourth edition (Academic Press, an imprint of Elsevier).
64. Diepart, C., Verrax, J., Calderon, P.B., Feron, O., Jordan, B.F., and Gallez, B. (2010). Comparison of methods for measuring oxygen consumption in tumor cells in vitro. Anal. Biochem. *396*, 250–256. https://doi.org/10.1016/j.ab.2009.09.029.
65. Baras, A.S., Mitchell, C.J., Myers, J.R., Gupta, S., Weng, L.C., Ashton, J.M., Cornish, T.C., Pandey, A., and Halushka, M.K. (2015). miRge - A Multiplexed Method of Processing Small RNA-Seq Data to Determine MicroRNA Entropy. PLoS One *10*, e0143066. https://doi.org/10.1371/journal.pone.0143066.
66. Mjelle, R., Aass, K.R., Sjursen, W., Hofsli, E., and Sætrom, P. (2020). sMETASeq: Combined Profiling of Microbiota and Host Small RNAs. iScience *23*, 101131. https://doi.org/10.1016/j.isci.2020.101131.

STAR★METHODS

KEY RESOURCES TABLE

REAGENT or RESOURCE	SOURCE	IDENTIFIER
Antibodies		
Anti-TNF-a Rabbit polyclonal antibody	ServiceBio	Cat# GB11188; RRID: AB_3075517
Rabbit Anti-Parvalbumin Polyclonal Antibody, Unconjugated	Abcam	Cat# ab11427; RRID: AB_298032
Anti-IL-17 Rabbit polyclonal antibody	ServiceBio	Cat# GB11110-1; RRID: AB_2892098
Anti-GFAP antibody	Abcam	Cat# ab7260; RRID: AB_305808
Chemicals, peptides, and recombinant proteins		
ApopTag® Plus Peroxidase *in Situ* Apoptosis Kit	Sigma-Aldrich	Cat# S7101
Direct-zol RNA Microprep Kits	Zymo research	Cat# R2062
TURBO DNA-free™ Kit	Thermo Fisher	Cat# AM1907
TRIzol™ Reagent	Thermo Fisher	Cat# 15596026
Experimental models: Organisms/strains		
Mice: C57BL/6J	Charles River Laboratories	Strain Code:027 RRID: IMSR_CRL:027
Software and algorithms		
CaseViewer Image Browser 2.4 edition	3D HISTECH	https://www.3dhistech.com/solutions/caseviewer/
Prism	GraphPad	https://www.graphpad.com/scientific-software/prism/
ImageJ	NIH	https://imagej.nih.gov/ij/index.html
Deposited data		
RNA-seq data of murine cerebellar tissue	This paper	SRA: PRJNA1134215

RESOURCE AVAILABILITY

Lead contact

Further information and requests for resources and reagents should be directed to and will be fulfilled by the lead contact, Ioannis Koutroulis MD, PhD, MBA ikoutrouli@childrensnational.org, ikoutroulis@gwu.edu.

Materials availability

MSC-derived sEVs were isolated from human adipose-derived MSC cell cultures (ADMSC) obtained from Zen-Bio (Durham, NC) for the purpose of this research.

Data and code availability

- RNA-seq data from murine cerebellar tissue of control, septic, and treated samples have been deposited in the NCBI SRA repository and are publicly available. The accession number is listed in the key resources table.
- This paper does not report original code.
- Any additional information required to reanalyze the data reported in this paper is available from the lead contact upon request.

EXPERIMENTAL MODEL AND STUDY PARTICIPANT DETAILS

Wildtype male mice at 8–10 weeks of age ($n = 75$) C57BL/6 (Charles River Laboratories, strain code: 027) were maintained in the animal facility of the Children's National Hospital and handled in accordance with the Institutional Animal Care and Use Committee (IACUC #00030714) and the Use Committee of Children's National Hospital, who approved all the protocols and the Guide for the Care and Use of Laboratory Animals (National Institute of Health). Mice were maintained in the animal facility under a 12-h dark–light cycle, constant temperature (20–26°C) and humidity maintenance (40–60%), and access to food and water *ad libitum*.

METHOD DETAILS

Murine model of sepsis

Male mice at 8–10 weeks of age were randomly assigned to four groups:

- Control + media (n = 16): male mice received intraperitoneal (IP) injection of PBS and tail vein injection of EVs-depleted media after 6 h.
- Control + sEVs (n = 14): male mice received IP injection of PBS and tail vein injection with adipose tissue MSC-derived sEVs after 6 h.
- Sepsis + media (n = 19): male mice received IP injection of cecal slurry and tail vein injection with sEVs-depleted after 6 h.
- Sepsis + sEVs (n = 26): male mice received IP injection of cecal slurry and tail vein injection with MSC-derived sEVs after 6 h.

The cecal slurry mixture was made from the cecal contents of euthanized donor male mice. Mice were gently restrained using a mouse restrainer and the tail was immersed in warm water to promote vasodilation and aid in the identification of the lateral tail veins. Subsequently, a single dose of sEVs (10E+08 to 10E+09 particles in 250 μL), or sEV-depleted media that was used for MSC culture was administered intravenously via a lateral tail vein using a 28-gauge needle, 6 h post-cecal slurry injection. Injection of cecal slurry caused polymicrobial sepsis in the recipient mice. The cecal slurry model, based on our extensive experience and other studies, is an effective way to induce polymicrobial sepsis, while decreasing animal suffering and variability between animals. Mice were evaluated every 2 h and scored on the severity of disease progression, using a validated murine sepsis severity score by Shrum et al. that assesses general appearance, level of consciousness, activity level, response to stimulus, eyes appearance, respiratory rate and respiration quality. The maximum score is 28 as there are seven variables measured with five possible scores (0–4) for each variable. This scoring system has been proven to be reliable, sensitive, and specific and can aid in the comparison of disease outcomes and therapeutic regimens across multiple models of sepsis. It is also a basis for pathophysiologic analysis of disease. Mice were sacrificed when they received a sepsis score of 15 or higher on the scale ranging from 0 to 28 or at 24 h post-intraperitoneal injection. Brain tissue was harvested after perfusion with PBS at the time of euthanasia for further study. Harvested tissue was either used immediately after isolation or immersed in liquid nitrogen and stored in −80°C. The scoring system used in the experiments is depicted in Table 1.

Isolation and characterization MSC-derived sEVs

In our study, MSC-derived sEVs were isolated from human adipose-derived MSC cell cultures (ADMSC) obtained from Zen-Bio (Durham, NC). For isolation, 3000 mL of conditioned media from approximately 300 million cells underwent tangential flow filtration (TFF), followed by size exclusion chromatography (SEC) utilizing a 10 mL column with a 70 nm pore size. The isolated particles were then diluted in sterile Dulbecco's Phosphate Buffered Saline (DPBS). Quality assessment of the sEVs involved protein determination and approximate RNA concentration measurements, conducted using a Thermo NanoDrop spectrophotometer through direct absorbance, without lysing, staining, or extracting RNA from the exosomes. Furthermore, the diameter and concentration of the particles were determined by Nanoparticle Tracking Analysis (NTA) with a Particle Metrix ZetaView.Surface protein characterization of the sEVs, specifically for the tetraspanins CD81, CD63, and CD9, served as specific markers to confirm their identity which depicted the sEVs under an electron microscope (Figure S3A), which presented the high-throughput surface protein characterization of sEVs using beads conjugated with antibodies against CD81, CD63, and CD9 (Figure S3B).

Tissue processing and histological assessment

Septic or non-septic control mice were anesthetized with isoflurane and transcardially perfused with 0.1 M phosphate buffered saline (PBS), pH 7.4, followed by 4% paraformaldehyde (PFA). Brains were postfixed in 4% PFA overnight, and then stored in PBS at 4°C until further use. Neuropathological alterations in sepsis mice (n = 8) compared to non-septic controls (n = 7) were confirmed histologically by hematoxylin and eosin (H&E) stain, using a modified quality scoring system that was previously described (Hoque et al., 2014). Evaluation of the mouse histology slides was performed by two different investigators blinded to treatment. Morphological cell grading was carried out under light microscopy at 600× magnification using an oil immersion lens. Normal neurons were evaluated and scored using morphological criteria. This scoring system, ranging from 0 (no injury) to 4 (severe injury), provides an assessment of tissue injury based on morphological cellular changes associated with injury including nuclear pyknosis, cytoplasmic shrinkage, cytoplasmic micro-vacuolation, perineuronal edema, cell death, and chromatolysis. Antibodies against TNF-a (ServiceBio, GB11188, dilution 1:200), parvalbumin (PV) (Abcam, ab11427, dilution 1:100), IL-17a (ServiceBio, GB11110-1, dilution 1:200), GFAP (Abcam, ab7260, dilution 1:500) and appropriate secondary antibodies were used for immunofluorescent analysis. Sections adjacent to those stained with H&E and immunofluorescence were assessed for *in situ* DNA fragmentation using the terminal deoxyribonucleotidyl transferase (TdT)-mediated biotin-14-dUTP nick-end labeling (TUNEL) procedure (ApopTag plus peroxidase *in situ* apoptosis detection kit, Intergen, Purchase, NY). TUNEL staining was performed as described previously.[60]

Image acquisition and analysis

We used a BX43 Olympus microscope with a Hamamatsu monochrome camera and a DP23 Olympus camera for brightfield microscopy. Images were viewed using NIH ImageJ and the CaseViewer Image Browser 2.4 edition software. All histological quantifications were performed in a blinded manner. Neuropathology scoring[61] including cell death, vacuolization, PC pathology, GFAP+ and TUNEL+ cells were manually counted in each optical section using the ImageJ "Cell Counter" plugin at 40× per regions of interest with a perimeter of 1 mm.

To acquire full cerebellum views in low magnification, we used the PANNORAMIC MIDI II automatic digital slide scanner microscope from 3D Histech. We used the Point Gray GS3-U3-51S5M-C camera. z stack images of 1-μm-thick single planes were captured using the 3D histech

software version 1.23.1.71684. The camera adapter magnification was 0.63×, micrometer/pixel X: 0.273810, micrometer/pixel Y: 0.273810, output resolution: 36.521675. The low magnification images were taken at 1.4×. The cerebellum anatomy was identified according to the Allen Brain Atlas (mouse)[62] and Paxinos and Franklin's The Mouse Brain in Stereotaxic Coordinates.[63]

Data were obtained from eight mice per septic group with MSC-derived sEV treatment and seven mice for the control group for H&E and TUNEL staining. All histological quantifications were performed in a blinded manner. For the cytokine analysis six mice were used as controls, seven mice and eight mice for the sepsis-media group for TNF-α, PV and IL-17α respectively, and five mice and six mice for the sepsis- MSC-derived for TNF-α, PV and for IL-17α respectively.

OXPHOS assessment by seahorse in cerebellar samples

We isolated cerebellar tissue from mice in the treatment and control groups and immediately used it for metabolomics so there wouldn't be any changes in their metabolic phenotype. Tissue sections of 100-micron depth and 2 mm diameter were obtained and placed in artificial cerebrospinal fluid. Cerebellar tissue was then added to an islet capture microplate to be analyzed in the Seahorse XFe Analyzer© (Agilent, Santa Clara, CA) which is a powerful instrument used for measuring oxidative phosphorylation in the same sections. Using the Seahorse XFe Analyzer© we measured the major energy pathway of the cell (i.e., mitochondrial respiration) in brain tissue sections from septic mice exposed to MSC-derived sEVs. The Seahorse XFe Analyzer© utilizes inert optical microsensors to measure oxygen consumption rate (OCR).[64] OCR is indicative of mitochondrial consumption of oxygen in OXPHOS to generate ATP. There were four groups of mice in the study: septic treated with MSC-derived sEVs (n = 5), septic injected with sEV-depleted media (n = 6), controls treated with MSC-derived sEVs (n = 6) and controls injected with sEV-depleted media (n = 7). Group comparisons were done using ANOVA on ranks to determine significance of pairwise comparisons.

Cerebellar tissue RNA sequencing

Total RNA was isolated from brain sections from each sample using TRIzol (ThermoFisher Scientific, Waltham, MA) according to manufacturer's recommendations. Total sample RNA was treated with the TURBO DNA-free Kit (ThermoFisher Scientific, Waltham, MA) to remove any contaminating DNA. Approximately 500 ng of total RNA for each sample was sent to Penn State University for sequencing library preparation and RNA sequencing. The total RNA was prepped for sequencing using the Illumina TruSeq Stranded Total RNA Library Prep Kit with the Ribo-Zero Gold rRNA Removal Kit (Epidemiology). The resultant Illumina sequencing libraries was sequenced on an Illumina NovaSeq 6000 sequencer using a 150 bp paired-end run.

MSC-derived sEV miRNA sequencing

Total RNA was isolated from three samples of MSC-derived sEVs using Trizol LS reagent (ThermoFisher Scientific, Waltham, MA) in combination with the Direct-zol RNA Microprep Kit (Zymo Research, Irvine, CA). RNA quantity was measured with the Qubit 2.0 fluorometer (ThermoFisher Scientific, Waltham, MA) and RNA quality was assessed with the Agilent Bioanalyzer 2100 (Agilent, Palo Alto, CA) using the RNA 6000 Pico Kit. RNA was prepared at the University of Maryland for sequencing using the Illumina Small RNA-Seq Library prep kit (Illumina, San Diego, CA) and sequenced on an Illumina NovaSeq6000 sequencer using an S2 100 bp PE Flowcell (Illumina, San Diego, CA). miRNA detection and abundance were estimated in miRge3.0 and sMETASeq.[65,66] Fastq files underwent quality control in CUTEADAPT and collapse into unique reads. Files were annotated against multiple search libraries (mature miRNAs, miRNA hairpins, mRNAs, mature & primary tRNAs, snoRNAs, rRNAs, other non-coding RNA) in miRge3.0 and against the miRBase and RNACentral libraries in sMETASeq. Raw miRNA counts were estimated for each sample.

QUANTIFICATION AND STATISTICAL ANALYSIS

The number of animals utilized in each experimental group is specified within the legends of the respective figures. Data visualization, including the plotting of graphs and the calculation of standard error of the mean (±SEM), was performed using Prism software. This software was also employed to assess statistical significance across all datasets. Specifically, one-way ANOVA was utilized to analyze differences among groups for the sepsis severity score, neuropathology scoring, Seahorse assay data, GFAP and the inflammatory cytokine (TNF-α and IL-17α) quantification. For transcriptomic analysis, differential expression was ranked based on p-values obtained through Fisher's Exact Test. Visualization of these analyses was facilitated by coloring boxes in the heatmap according to z-scores, where red or green indicates activation and gray denotes inactivation.